Neutrino-nucleus scattering off ^{136}Xe

E. Ydrefors,[1,*] J. Suhonen,[2] and Y. M. Zhao[1,3]

[1]*Department of Physics and Astronomy, and Shanghai Key Laboratory for Particle Physics and Cosmology, Shanghai Jiao Tong University, Shanghai 200240, China*

[2]*Department of Physics, University of Jyväskylä, Jyväskylä FI-40014, Finland*

[3]*IFSA Collaborative Innovation Center, Shanghai Jiao Tong University, Shanghai 200240, China*

(Received 24 October 2014; revised manuscript received 10 December 2014; published 9 January 2015)

Background: Theoretical estimates of the cross sections for the neutrino-nucleus scattering off relevant nuclei for supernova neutrinos are essential for many applications in neutrino physics and astrophysics. The double-β-decaying nucleus ^{136}Xe nucleus is used by the EXO Collaboration in the search for neutrinoless double-β decay. A ton-scale experiment based on ^{136}Xe could also be used for studies of supernova neutrinos and/or solar neutrinos.

Purpose: The purpose of the present work is, thus, to perform a study of the charged-current and neutral-current nuclear responses to supernova neutrinos for ^{136}Xe.

Method: The cross sections are computed by using the well-established framework for studies of semileptonic processes in nuclei introduced by O'Connell, Donnelly, and Walecka [Phys. Rev. C **6**, 719 (1972)]. The nuclear wave functions of the initial and the final nuclear states for the neutral-current neutrino-nucleus scattering in ^{136}Xe are computed by using the quasiparticle random-phase approximation (QRPA). Similarly, the pnQRPA is adopted to construct the initial and final nuclear states which are relevant for the charged-current reactions. The nuclear responses to supernova neutrinos are subsequently computed by folding the cross sections with appropriate energy spectra for the incoming neutrinos.

Results: We present results for the cross sections of the charged-current and neutral-current neutrino and antineutrino scatterings off ^{136}Xe. Nuclear responses to supernova neutrinos are also given. For the considered scenario for the neutrino mixing we have found that neutrino interactions with matter and so-called collective neutrino oscillations enhance significantly the neutrino and antineutrino flux-averaged cross sections.

Conclusions: We have found that for the charged-current and neutral-current neutrino scatterings off ^{136}Xe transitions mediated by the 1^+ multipole are the most important ones. However, for the charged-current antineutrino channel 0^+ and 1^+ transitions are largely suppressed due to the large neutron excess. Transitions to 1^- and 2^- final nuclear states are thus relatively more important for the charged-current antineutrino scattering.

DOI: 10.1103/PhysRevC.91.014307 PACS number(s): 25.30.Pt, 21.60.−n, 23.40.Bw

I. INTRODUCTION

Supernova neutrinos constitute very valuable probes of physics beyond the standard model [1,2] and the currently unknown supernova mechanisms [3]. One of the currently unanswered questions in neutrino physics is whether the neutrino mass hierarchy is normal or inverted. The signal produced in a large-scale detector by a future nearby supernova could probably be used to disentangle this important question [4,5]. Furthermore, recent simulations [6] show that supernova neutrinos could undergo so-called collective neutrino-neutrino oscillations.

From the astrophysical side, nuclear weak interactions play prominent roles during almost all stages of a supernova explosion [7]. Supernovae also constitute one of the proposed sites of the r-process. Neutrino-nucleus reactions would in that case play a paramount role for the nucleosynthesis of the heavy elements [8].

Neutrinos from astrophysical sources (e.g., supernovae or the sun) can be studied by using earth-bound detectors. Examples of existing and planned detectors are the Helium and Lead Observatory (HALO) [9], the Majorana/Mo Observatory Of Neutrinos (MOON) [10], and the Hyper-Kamiokande (Hyper-K) [11]. Theoretical estimates of neutrino-nucleus cross sections are very important for the interpretation of the results of such measurements. Nuclear responses to supernova neutrinos also constitute important inputs in supernova simulations.

The studies of the neutrinoless double-β ($0\nu\beta\beta$) decay of a suitable set of even-even nuclei constitute a realistic way to determine the absolute mass spectrum of neutrinos [12]. Furthermore, an observation of the $0\nu\beta\beta$ decay would also confirm that the neutrino is a Majorana particle. One currently running experiment with such aims is the EXO (Enriched Xenon Observatory [13]), which is using ^{136}Xe. A ton-scale double-β-decay experiment based on ^{136}Xe such as the proposed nEXO [14] could also be used for studies of neutrinos from astrophysicsal sources such as supernovae or the sun.

In this paper we therefore perform a study of the cross sections for the charged-current (CC) and neutral-current (NC) neutrino-nucleus scatterings off ^{136}Xe for energies of the incoming neutrino which are relevant for supernova neutrinos. The nuclear responses to supernova neutrinos are also estimated by folding the cross sections with appropriate energy spectra of the incoming neutrinos.

The computations which are pursued in this paper are based on the Donnelly-Walecka formalism [15]. In previous works we have used the aforementioned theory to study the

*ydrefors@kth.se

charged-current and neutral-current neutrino cross sections for the even-even [16,17] and the odd-mass Mo isotopes [18] and ^{116}Cd [19]. In the present work we adopt the quasiparticle random-phase approximation (QRPA; see, e.g., Ref. [20]) to construct the final and initial states for the NC reactions and the pnQRPA for the CC reactions in ^{136}Xe.

For medium-heavy and heavy even-even nuclei, the cross sections for the charged-current neutrino-nucleus scattering are dominated by transitions to 1^+ final states in the corresponding odd-odd nucleus (i.e., ^{136}Cs in the present work). One problem in the pnQRPA calculations of 1^+ states in odd-odd nuclei is the unsettled value of the $g_{\rm pp}$ parameter which determines the strength of the particle-particle part of the proton-neutron interaction. This issue, which also is very important for calculations of nuclear matrix elements related to $0\nu\beta\beta$ decay, has been discussed in great detail in Ref. [21]. Therefore, in the present work the dependence of the computed neutrino-nucleus cross sections on the particle-particle strength is also studied.

This paper is organized as follows. In Sec. II we summarize the QRPA and the pnQRPA. The formalism for the calculation of neutrino-nucleus cross sections is also briefly discussed. Then, in Sec. III we discuss our results. Finally, in Sec. V we draw our conclusions.

II. THEORY

A. QRPA and pnQRPA

In this work the required wave functions of the nuclear states in ^{136}Xe are constructed by using the QRPA. Similarly, the pnQRPA is adopted to compute the nuclear states in the β-decay partners ^{136}Cs and ^{136}I. Therefore, in this section the formalisms of these models are briefly summarized. A more detailed treatment can be found in, e.g., Ref. [20].

In the present calculations the quasiparticles are treated in the BCS theory. The starting point is then the variatonal ansatz for the BCS ground state

$$|\text{BCS}\rangle = \prod_{\alpha>0}(u_a - v_a c_\alpha^\dagger \tilde{c}_\alpha^\dagger)|\text{CORE}\rangle, \tag{1}$$

where $|\text{CORE}\rangle$ represents the core. In Eq. (1) the index a holds the single-particle quantum numbers n_a,l_a, and j_a. The index α includes in addition the magnetic quantum number m_α, i.e., $\alpha = (a,m_\alpha)$. Here $c_\alpha^\dagger$ denotes the particle creation operator and $\tilde{c}_\alpha$ is the corresponding time-reversed particle annihilation operator, which is defined as $\tilde{c}_\alpha = (-1)^{j_a+m_\alpha} c_{-\alpha}$ with $-\alpha = (a,-m_\alpha)$.

The quasiparticles are subsequently defined via the Bogoliubov-Valatin transformation as

$$a_\alpha^\dagger = u_a c_\alpha^\dagger + v_a \tilde{c}_\alpha, \quad \tilde{a}_\alpha = u_a \tilde{c}_\alpha - v_a c_a^\dagger. \tag{2}$$

In the QRPA the states are formed by coupling two-quasiparticle operators to good angular momentum J_ω and parity π_ω. An excitation $\omega = (J_\omega,\pi_\omega,k_\omega)$ of the even-even nucleus under consideration is thus obtained by using the creation operator

$$Q_\omega^\dagger = \sum_{a\le a'} \sigma_{aa'}^{-1}\left(X_{aa'}^\omega [a_a^\dagger a_{a'}^\dagger]_{J_\omega M_\omega} + Y_{aa'}^\omega [\tilde{a}_a \tilde{a}_{a'}]_{J_\omega M_\omega}\right), \tag{3}$$

where $\sigma_{aa'} = \sqrt{1+\delta_{aa'}}$ and the sum is over all proton-proton and neutron-neutron configurations such that none of them are counted twice. Here the quantum number k_ω enumerates states having the same angular momentum and parity.

Similarly, in the pnQRPA the creation operator has the form

$$Q_\omega^\dagger = \sum_{pn}\left(X_{pn}^\omega [a_p^\dagger a_n^\dagger]_{J_\omega M_\omega} + Y_{pn}^\omega [\tilde{a}_p \tilde{a}_n]_{J_\omega M_\omega}\right). \tag{4}$$

In both the QRPA and the pnQRPA the required amplitudes X^ω and Y^ω can be solved from the matrix equation

$$\begin{pmatrix} A & B \\ -B^* & -A^* \end{pmatrix}\begin{pmatrix} X^\omega \\ Y^\omega \end{pmatrix} = E_\omega \begin{pmatrix} X^\omega \\ Y^\omega \end{pmatrix}, \tag{5}$$

where E_ω denotes the energy of the excitation ω. Here A is the (pn)QTDA matrix and the matrix B contains the ground-state correlations.

B. Neutrino-nucleus scattering

In this work we are interested in the following charged-current processes

$$\nu_l + (A,Z) \longrightarrow (A,Z+1) + l^-, \tag{6}$$

$$\bar{\nu}_l + (A,Z) \longrightarrow (A,Z-1) + l^+, \tag{7}$$

and the neutral-current proccesses

$$\nu_l + (A,Z) \longrightarrow (A,Z)^* + \nu_l, \tag{8}$$

$$\bar{\nu}_l + (A,Z) \longrightarrow (A,Z)^* + \bar{\nu}_l, \tag{9}$$

where $l = \text{e},\mu,\tau$. In the charged-current reactions (6) and (7) the final nuclear state is either the ground state or an excited state in the corresponding odd-odd nucleus. But, in the incoherent reactions (8) and (9), the final nuclear state is an excited state in ^{136}Xe.

In the present work the four-momentum transfer for the (anti)neutrino is defined as

$$q_\kappa = k'_\kappa - k_\kappa = p_\kappa - p'_\kappa, \tag{10}$$

where k_κ (k'_κ) denotes the four-momentum of the incoming (outgoing) lepton, and p_κ and p'_κ are the four-momenta of the initial and final nuclei. We follow here the same conventions as in Ref. [22]. The four-momentum of the incoming lepton is thus defined as $k_\kappa = (E_{\mathbf{k}}, -\mathbf{k})$ and the four-momentum of the outgoing lepton as $k'_\kappa = (E_{\mathbf{k}'}, -\mathbf{k}')$. The four-momenta p_κ and p'_κ of the initial and final nuclei are defined similarly.

We assume that the final and initial nuclear states have well-defined angular momenta and parities. The double-differential cross section for the neutrino-nucleus scattering from an initial nuclear state (i) (with angular momentum J_i) to a final nuclear state (f) (with angular momentum J_f) can then be expressed in the form [16]

$$\left(\frac{d^2\sigma_{i\longrightarrow f}}{d\Omega \mathrm{d}E_{\rm exc}}\right)_{\nu/\bar{\nu}} = \frac{G^2 F(\pm Z_f, E_{\mathbf{k}'})|\mathbf{k}'|E_{\mathbf{k}'}}{\pi(2J_i+1)} \times \left(\sum_J \sigma_{\rm CL}^J + \sum_{J\ge 1}\sigma_{\rm T}^J\right), \tag{11}$$

where the Coulomb-longitudinal and transverse components are defined as

$$\sigma_{\rm CL}^{J} = (1 + a\cos\theta)|(J_f\|\mathcal{M}_J(q)\|J_i)|^2 + (1 + a\cos\theta - 2b\sin^2\theta)|(J_f\|\mathcal{L}_J(q)\|J_i)|^2 + \frac{E_{\rm exc}}{q}(1 + a\cos\theta + c)2{\rm Re}[(J_f\|\mathcal{L}_J(q)\|J_i)(J_f\|\mathcal{M}_J(q)\|J_i)^*] \quad (12)$$

and

$$\sigma_{\rm T}^{J} = (1 - a\cos\theta + b\sin^2\theta)\left[\left|\left(J_f\left\|\mathcal{T}_J^{\rm mag}(q)\right\|J_i\right)\right|^2 + \left|\left(J_f\left\|\mathcal{T}_J^{\rm el}(q)\right\|J_i\right)\right|^2\right] \mp \frac{E_{\mathbf{k}} + E_{\mathbf{k}'}}{q}(1 - a\cos\theta - c) \times 2{\rm Re}\left[\left(J_f\left\|\mathcal{T}_J^{\rm mag}(q)\right\|J_i\right)\left(J_f\left\|\mathcal{T}_J^{\rm el}(q)\right\|J_i\right)^*\right]. \quad (13)$$

Here the excitation energy $E_{\rm exc}$ of the final nuclear state is defined with respect to the ground state of the initial nuclear state and thus $E_{\rm exc} = E_{\mathbf{p}'} - E_{\mathbf{p}}$. For the neutral-current neutrino-nucleus scatterings the effective weak coupling constant is $G = G_{\rm F}$ where $G_{\rm F}$ denotes the Fermi coupling constant. However, for the charged-current processes a slightly modified value of $G = \cos\theta_{\rm C} G_{\rm F}$ is used where $\theta_{\rm C}$ represents the Cabibbo angle. In Eqs. (12) and (13) we have also used the abbreviations

$$a = \sqrt{1 - (m_l/E_{\mathbf{k}'})^2}, \quad (14)$$

$$b = \frac{a^2 E_{\mathbf{k}} E_{\mathbf{k}'}}{q^2}, \quad (15)$$

and

$$c = \frac{m_l^2}{q E_{\mathbf{k}'}}, \quad (16)$$

where m_l represents the rest mass of the outgoing lepton and the magnitude of the three-momentum transfer is given by

$$q = |\mathbf{q}| = \sqrt{a^2 E_{\mathbf{k}'}^2 + E_{\mathbf{k}}^2 - 2a E_{\mathbf{k}'} E_{\mathbf{k}'}\cos\theta}, \quad (17)$$

where θ denotes the angle between the incoming and outgoing leptons. Furthermore, in Eq. (13) the $-$ $(+)$ sign is used for neutrinos (antineutrinos).

In the calculations of charged-current (anti) neutrino scattering off nuclei it is important to properly take into account the Coulomb distortion of the wave function of the outgoing lepton. This is in Eq. (11) associated with the function $F(\pm Z_f, E_{\mathbf{k}'})$. This effect has to be treated differently in the regions of small and large values of the so-called effective momentum of the outgoing lepton. This effective momentum is defined as

$$k_{\rm eff} = \sqrt{E_{\rm eff}^2 - m_l^2}, \quad (18)$$

where the effective energy of the outgoing lepton is given by

$$E_{\rm eff} = E_{\mathbf{k}'} - V_{\rm C}(0). \quad (19)$$

In Eq. (19) $V_{\rm C}(0)$ represents the value at the origin of the Coulomb potential produced by the final nucleus. For small values of $k_{\rm eff}$, i.e., $k_{\rm eff} R \ll 1$, we use in Eq. (11) a Fermi function. In the region of large values of the effective momentum we adopt the so-called modified effective momentum approximation which was introduced in Ref. [23]. Consequently, we put $F(\pm Z_f, E_{\mathbf{k}'}) = 1$ and the absolute value of the three-momentum and the energy of the outgoing lepton are replaced by their effective values given by Eqs. (18) and (19), respectively. For more details we refer to Ref. [16]. Furthermore, for the neutral-current reactions (8) and (9) the outgoing lepton has no charge and thus the value $F(\pm Z_f, E_{\mathbf{k}'}) = 1$ is used.

The nuclear-structure dependence of the cross sections is contained in the nuclear matrix elements of the operators $\mathcal{M}_J(q), \mathcal{L}_J(q), \mathcal{T}_J^{\rm mag}(q)$, and $\mathcal{T}_J^{\rm el}(q)$. The definitions of these operators are given in Ref. [24]. The aforementioned operators depend on the nucleon form factors $F_{1,2}^V(Q^2)$ (vector), $F^A(Q^2)$ (axial-vector), and $F^P(Q^2)$ (pseudo-scalar), which depend on the four-momentum transfer $Q^2 = -q_\kappa q^\kappa$. In the present calculations we adopt the expressions for the neutral-current and charged-current form factors, which are discussed in Refs. [22] and [16] respectively. Hence, the axial-vector form factor $F^A(Q^2)$ is of the dipole-form with the static value $F^A(0) = -1.0$.

III. RESULTS

A. Nuclear structure

In the present computations we adopted a large valence space consisting of the complete $3\hbar\omega$,$4\hbar\omega$, and $5\hbar\omega$ main harmonic oscillator shells plus the $0i_{13/2}$ and $0i_{11/2}$ orbitals for both protons and neutrons. The single-particle energies were first generated by using a Coulomb-corrected Woods-Saxon potential with the parametrization of Ref. [25]. In the calculations the Bonn one-boson exchange potential [26] was used as the two-body interaction. BCS calculations were then performed for protons and neutrons separately. For protons the monopole matrix elements were scaled by a common factor $g_{\rm p}^{\rm pair}$ such that the empirical pairing gap computed from the three-point formulas (see, e.g., Ref. [20]) was reproduced. This procedure cannot be used on the neutron side since ^{136}Xe is neutron magic. In the present calculations we have therefore used the unscaled value $g_{\rm n}^{\rm pair} = 1.0$ for the neutrons. This means that the particle-hole case is recovered, i.e., $u_a = 0$ $(u_a = 1)$ and $v_a = 1$ $(v_a = 0)$ for the neutron orbitals below (above) the Fermi surface $N = 82$. In the computations the single-particle energies for the orbitals close to the respective Fermi surfaces were slightly adjusted in order to improve the agreement with the experimental data. These adjusted single-particle energies are compared with the Woods-Saxon energies in Table I.

In the QRPA calculations of the states in ^{136}Xe the two-body matrix elements for the particle-particle and particle-hole

TABLE I. Woods-Saxon energies and adjusted single-particle energies for neutrons (ν) and protons (π), respectively.

Orbital	E_{WS}	E_{adj}
$\nu 0g_{7/2}$	−10.92	−9.97
$\nu 1d_{5/2}$	−10.89	−10.10
$\nu 1d_{3/2}$	−8.84	−8.84
$\nu 2s_{1/2}$	−9.06	−9.13
$\nu 0h_{11/2}$	−7.98	−9.37
$\nu 0h_{9/2}$	−2.03	−2.42
$\nu 1f_{5/2}$	−0.84	−2.34
$\nu 2p_{3/2}$	−2.14	−3.04
$\nu 2p_{1/2}$	−1.26	−2.65
$\pi 0g_{7/2}$	−7.42	−8.42

channels were scaled by the constants g_{pp} and g_{ph}, respectively. This was done for each multipole J^{π} separately in such a way that the low-lying experimental energy spectrum of ^{136}Xe was reproduced as well as possible. The QRPA method leads to a spurious 0^{+}_{1} state which can be removed by setting its energy to zero by adjusting the particle-hole strength of the 0^{+} channel and simultaneously fixing g_{pp} such that the energies of the low-lying one-phonon states are roughly reproduced. Furthermore, the lowest 1^{-}_{1} state is spurious because of center-of-mass motion. In the present computations the particle-hole strength of the 1^{-} channel has thus been adjusted in such a way that the energy of the lowest 1^{-} solution is brought to zero and subsequently the state is removed from the calculations. The adjusted values of the QRPA parameters are displayed in Table II. For the other multipoles the unscaled values $g_{\mathrm{pp}} = 1.0$ and $g_{\mathrm{ph}} = 1.0$ have been used.

Similarly, pnQRPA calculations were performed for the states in the odd-mass nuclei ^{136}Cs and ^{136}I. But in this case only the particle-particle and particle-hole strengths of the 1^{+} channel were adjusted. The parameter g_{ph} was then adjusted in order to reproduce the energy of the giant Gamow-Teller resonance, i.e., $E \approx 15.0$ MeV [27]. As was discussed in Sec. I the value of the particle-particle strength is more difficult to determine. In Ref. [21,28] an average value of $g_{\mathrm{pp}} = 0.63$ was determined and used based on $2\nu\beta\beta$ half-lives and comparative half-lives of single-β decays. Therefore in this work we have performed pnQRPA calculations for two sets of pnQRPA parameters: A set (called I) in which the unscaled value $g_{\mathrm{pp}} = 1.00$ was used and a second one (II) in which $g_{\mathrm{pp}} = 0.60$ was used. In both of the calculations the value of g_{ph} was fixed according to the procedure described above. The two sets of pnQRPA parameters are presented in Table III.

Unfortunately, the pnQRPA computed energy of the isoscalar analog state is much too small compared to the experimental energy. No reasonable value of the particle-hole strength could be found for which the measured energy of $E = 13.38$ MeV [27] is reproduced. This problem is explained by the fact that the present calculations are lacking self-consistency because of the use of a Woods-Saxon mean field. In self-consistent Skyrme calculations, such as the ones which were performed in Ref. [29] for ^{116}Cd, the energy of the isobaric analog state is correctly reproduced. Therefore, in the present computations the energy of the corresponding pnQRPA state has been set to the experimental value by hand.

TABLE II. Adopted values of the QRPA parameters g_{pp} and g_{ph} for the different multipoles J^{π}.

J^{π}	0^{+}	1^{-}	2^{+}	3^{-}	4^{+}	6^{+}
g_{pp}	0.89	1.00	1.00	1.00	1.00	1.00
g_{ph}	0.10	0.52	0.62	0.66	0.70	0.90

TABLE III. Adopted values of the pnQRPA parameters g_{pp} and g_{ph} in the 1^{+} channel. For more information we refer to the text.

Parameter set	$g_{\mathrm{pp}}(1^{+})$	$g_{\mathrm{ph}}(1^{+})$
I	1.00	1.20
II	0.60	1.18

IV. NEUTRINO CROSS SECTIONS

In the next step of our work we computed the cross sections for the charged-current and neutral-current (anti)neutrino scatterings off ^{136}Xe. The double-differential cross section for each final nuclear state f, scattering angle θ, and energy of the incoming neutrino $E_{\mathbf{k}}$ was then computed by using Eq. (11). The total cross section $\sigma(E_{\mathbf{k}})$ as a function of the neutrino energy $E_{\mathbf{k}}$ was subsequently calculated by integrating over the scattering angle θ and summing up the contributions coming from each final nuclear state. For more details, see Ref. [17].

The computed cross sections for the neutral-current reactions (8) and (9) are displayed in Table IV. Similarly, we show in Table V the results for the charged-current neutrino and antineutrino scatterings. In Table V $\sigma_{\nu}^{I}(\sigma_{\bar{\nu}}^{I})$ and $\sigma_{\nu}^{II}(\sigma_{\bar{\nu}}^{II})$ are the cross sections for the (anti)neutrino scatterings corresponding to the pnQRPA calculations I and II of Table III. It is seen in the aforementioned tables that, as expected, the cross sections for both the neutral-current and

TABLE IV. Computed cross sections for the neutral-current neutrino and antineutrino scatterings off ^{136}Xe in units of 10^{-42} cm^2 as functions of the energy of the incoming neutrino (antineutrino).

E_{ν}	$\sigma_{\nu}(E_{\nu})$	$\sigma_{\bar{\nu}}(E_{\nu})$
5.0	1.32 (−5)	1.29 (−5)
10.0	4.60 (−1)	4.46 (−1)
15.0	6.32 (0)	6.02 (0)
20.0	2.01 (1)	1.87 (1)
25.0	4.47 (1)	4.04 (1)
30.0	8.39 (1)	7.32 (1)
40.0	2.20 (2)	1.78 (2)
50.0	4.44 (2)	3.37 (2)
60.0	7.56 (2)	5.42 (2
70.0	1.14 (3)	7.82 (2)
80.0	1.59 (3)	1.05 (3
90.0	2.08 (3)	1.32 (3)
100.0	2.60 (3)	1.59 (3)

TABLE V. Computed cross sections for the charged-current neutrino and antineutrino scattterings off ^{136}Xe in units of 10^{-40} cm^2 as functions of the energy of the incoming neutrino (antineutrino). In the table are shown results for the two sets of pnQRPA parameters given in Table III.

E_ν	$\sigma_\nu^I(E_\nu)$	$\sigma_{\bar\nu}^I(E_\nu)$	$\sigma_\nu^{II}(E_\nu)$	$\sigma_{\bar\nu}^{II}(E_\nu)$
5.0	3.70 (−2)		2.62 (−2)	
10.0	3.20 (−1)	2.41 (−5)	2.79 (−1)	2.41 (−5)
15.0	1.30 (0)	5.98 (−4)	1.20 (0)	7.22 (−4)
20.0	4.38 (0)	4.22 (−3)	4.27 (0)	4.66 (−3)
25.0	9.82 (0)	1.53 (−2)	9.74 (0)	1.61 (−2)
30.0	1.69 (1)	3.89 (−2)	1.68 (1)	4.00 (−2)
40.0	3.38 (1)	1.46 (−1)	3.38 (1)	1.48 (−1)
50.0	5.55 (1)	3.78 (−1)	5.55 (1)	3.81 (−1)
60.0	7.98 (1)	8.62 (−1)	7.98 (1)	8.66 (−1)
70.0	1.05 (2)	1.74 (0)	1.05 (2)	1.75 (0)
80.0	1.31 (2)	3.08 (0)	1.31 (2)	3.09 (0)
90.0	1.58 (2)	4.72 (0)	1.58 (2)	4.73 (0)
100.0	1.84 (2)	6.52 (0)	1.84 (2)	6.53 (0)

charged-current processes increase strongly with increasing neutrino energy. From Table V we can conclude that for the charged-current reactions the cross sections for neutrinos are much larger than the ones for antineutrinos. Furthermore, the results in Table V for the two pnQRPA calculations of Table III (I and II) show that the value of the particle-particle strength ($g_{\rm pp}$) is rather important for low-energy neutrinos (i.e., for energies $E_{\mathbf{k}} \lesssim 10$ MeV). However, for energies of the incoming neutrino (or antineutrino) which are larger than 10 MeV the cross sections are not very sensitive to the adopted value of $g_{\rm pp}$.

One important quantity from the experimental point of view is the flux-averaged cross section, $\langle\sigma\rangle$, which is computed by folding the cross section $\sigma(E_{\mathbf{k}})$ with an appropriate energy spectrum for the incoming neutrinos. The energies of supernova neutrinos can rather well be described by a two-parameter Fermi-Dirac distribution

$$n_{\rm FD}(E_{\mathbf{k}}) = \frac{1}{F_2(\alpha_\nu)T_\nu}\frac{(E_{\mathbf{k}}/T_\nu)^2}{1+{\rm e}^{E_{\mathbf{k}}/T_\nu-\alpha_\nu}}, \tag{20}$$

where T_ν is the effective neutrino temperature and α_ν represents the so-called pinching parameter. A similar distribution is valid for antineutrinos by replacing ν by $\bar\nu$. Here the constant $F_2(\alpha_\nu)$ is chosen such that the total flux is normalized to unity.

In the present calculations we have adopted the neutrino parameters which are given in Table VI. In the table the neutrino temperature T_ν has been computed for each value of α_ν and average neutrino energy $\langle E_{\mathbf{k}}\rangle$ by using the relation

$$\langle E_{\mathbf{k}}\rangle/T_\nu = \frac{F_3(\alpha_\nu)}{F_2(\alpha_\nu)}, \tag{21}$$

with

$$F_k(\alpha_\nu) = \int \frac{x^k dx}{1+e^{x-\alpha_\nu}}. \tag{22}$$

TABLE VI. Adopted values of the parameters α_ν and $\langle E_{\mathbf{k}}\rangle$ for the different neutrino flavors. The corresponding neutrino temperatures computed from Eq. (21) are also shown. Here x $= \mu,\tau$ is a common label for the nonelectron flavors.

Flavor	α_ν	$\langle E_{\mathbf{k}}\rangle$	T_ν
$\nu_{\rm e}$	3.0	11.5	2.88
$\bar\nu_{\rm e}$	3.0	13.6	3.41
$\nu_{\rm x}$	0.0	16.3	5.17
$\bar\nu_{\rm x}$	0.0	16.3	5.17

In Table VII we display our QRPA calculated averaged cross sections for the neutral-current neutrino and antineutrino scatterings off ^{136}Xe. It is clearly seen from Table VII and Table VI that the average cross sections increase significantly with increasing average neutrino energy $\langle E_{\mathbf{k}}\rangle$. This is in agreement with results which have been found for other nuclear systems; see, e.g., Refs. [17,19].

Due to the large μ and τ rest masses only electron neutrinos (or antineutrinos) can be detected by using the charged-current reactions (6) and (7). However, the energy spectra for the incoming neutrinos can be modified significantly by neutrino-flavor transformations. The description of neutrino-flavor conversions under supernova conditions constitutes a nontrivial problem and involve neutrino-matter interactions, collective neutrino oscillations, and shock-wave effects. Furthermore, many of the details concerning neutrino mixing in supernovae are not yet fully understood. For more details on neutrino-flavor transformations in supernovae, we refer to Refs. [30,31].

For simplicity we limit ourselves in the present work to a specific case where the collective neutrino oscillations are not suppressed by the neutrino-matter interactions, i.e., the matter density is not too large in the collective regime. Furthermore, we assume that the matter is dense enough so that the Mikheev-Smirnov-Wolfenstein (MSW) resonances occur at large distances. Under these assumptions the collective oscillations and the neutrino-matter interactions can be treated independently. We also presume that the MSW H resonance is fully adiabatic, i.e., $P_{\rm H} = 0$. Consequently, we neglect possible effects coming from turbulence and/or shock-wave propagations which could make the H-resonance nonadiabatic.

Muon and τ neutrinos are believed to experience similar interactions in the supernova environment and are almost maximally mixed in vacuum. Therefore, it is adequate to only consider two-neutrino mixing of the form $\nu_y \leftrightarrow \nu_{\rm e}$, where ν_y denotes a linear combination of ν_μ and ν_τ. The energy spectra for electron neutrinos and electron antineutrinos after flavor

TABLE VII. Averaged cross sections for the neutral-current neutrino and antineutrino scatterings off ^{136}Xe in units of 10^{-42} cm^2.

$\nu_{\rm e}$	$\bar\nu_{\rm e}$	$\nu_{\rm x}$	$\bar\nu_{\rm x}$
5.31	9.30	26.5	22.6

TABLE VIII. Averaged cross sections for the charged-current neutrino and antineutrino scatterings off ^{136}Xe in units of 10^{-40} cm^2 computed for the two sets of pnQRPA parameters shown in Table III. In the table results are given for the nonoscillating case and for neutrinos which undergo neutrino-flavor transformations in the normal (NH) and inverted (IH) mass hierarchies, respectively.

	ν_e	ν_{ey}^{NH}	ν_{ey}^{IH}	$\bar{\nu}_e$	$\bar{\nu}_{ey}^{NH}$	$\bar{\nu}_{ey}^{IH}$
pnQRPA I	1.21	4.87	4.86	3.24×10^{-3}	1.40×10^{-2}	6.57×10^{-3}
pnQRPA II	1.16	4.82	4.80	3.41×10^{-3}	1.43×10^{-2}	6.80×10^{-3}

conversions are then given by

$$F_{\nu_e}(E_\mathbf{k}) = p(E_\mathbf{k})F^0_{\nu_e}(E_\mathbf{k}) + [1 - p(E_\mathbf{k})]F^0_{\nu_y}(E_\mathbf{k}) = p(E_\mathbf{k})F^0_{\nu_e}(E_\mathbf{k}) + [1 - p(E_\mathbf{k})]F^0_{\nu_x}(E_\mathbf{k}), \quad (23)$$

and

$$F_{\bar{\nu}_e}(E_\mathbf{k}) = \bar{p}(E_\mathbf{k})F^0_{\bar{\nu}_e}(E_\mathbf{k}) + [1 - \bar{p}(E_\mathbf{k})]F^0_{\bar{\nu}_y}(E_\mathbf{k}) = \bar{p}(E_\mathbf{k})F^0_{\bar{\nu}_e}(E_\mathbf{k}) + [1 - \bar{p}(E_\mathbf{k})]F^0_{\bar{\nu}_x}(E_\mathbf{k}), \quad (24)$$

where $F^0_{\nu_e}(E_\mathbf{k})[F^0_{\nu_x}(E_\mathbf{k})]$ and $F^0_{\bar{\nu}_e}(E_\mathbf{k})[F^0_{\bar{\nu}_x}(E_\mathbf{k})]$ are the initial energy distributions of electron neutrinos (nonelectron neutrinos) and electron antineutrinos (nonelectron antineutrinos), respectively. Equations (23) and (24) are valid for general energy profiles of supernova neutrinos. However, in the present work we adopt distributions of the form (20). Guided by Refs. [32,33] we use for the survival probability $p(E_\mathbf{k})$ $[\bar{p}(E_\mathbf{k})]$ of electron neutrinos (electron antineutrinos) in the case of normal mass hierarchy the prescriptions

$$p(E_\mathbf{k}) = 0, \quad (25)$$

and

$$\bar{p}(E_\mathbf{k}) = \begin{cases} \cos\theta_{12}; & E_\mathbf{k} < \bar{E}_s, \\ 0; & E_\mathbf{k} \geqslant \bar{E}_s, \end{cases} \quad (26)$$

with the split energy $\bar{E}_s = 18.0$ MeV. Furthermore, we adopt in the case of the inverted mass hierarchy the survival probabilities

$$p(E_\mathbf{k}) = \begin{cases} \sin^2\theta_{12}; & E_\mathbf{k} < E_s, \\ 0; & E_\mathbf{k} \geqslant E_s, \end{cases} \quad (27)$$

and

$$\bar{p}(E_\mathbf{k}) = \cos^2\theta_{12}, \quad (28)$$

where the split energy for neutrinos is $E_s = 7$ MeV.

However, it should be noticed that the collective effects on the survival probabilities are rather sensitive to the adopted supernova model; see, e.g., Ref. [34]. The prescriptions for p and $\bar{p}$ which are given by Eqs. (25)–(28) correspond thus only to one possible scenario.

In Table VIII we display our computed flux-averaged cross sections for the charged-current neutrino and antineutrino scatterings off ^{136}Xe. In the table ν_e ($\bar{\nu}_e$) denotes nonoscillating electron neutrinos (electron antineutrinos). Furthermore, we denote by ν_{ey}^{NH} ($\bar{\nu}_{ey}^{NH}$) and ν_{ey}^{IH} ($\bar{\nu}_{ey}^{IH}$) the electron neutrinos (electron antineutrinos) which have undergone flavor transformations for the normal and inverted mass hierarchy cases, respectively. It is seen in the table that the dependence of the average cross sections on the particle-particle strength is rather weak. The results which correspond to the two different values of g_{pp}, i.e., $g_{pp} = 1.0$ and $g_{pp} = 0.6$, differ by at most 5%. For the adopted prescriptions for p and $\bar{p}$ the cross sections for both the neutrino and antineutrino scatterings are enhanced significantly by neutrino-flavor transformations. Furthermore, our computed flux-averaged cross sections for the neutrino scattering are almost independent of the mass hierarchy. However, for the antineutrinos the results for the normal and inverted mass hierarchies differ significantly from each other. As mentioned above we consider here only a specific scenario for the neutrino-flavor transformations. The results in Table VIII should thus only be taken as an example of how the averaged cross sections could be changed by neutrino conversions which may occur under certain supernova conditions.

We have also studied the contributions coming from the leading multipole channels of Eq. (11) to the averaged cross sections for the CC and NC (anti)neutrino scatterings off ^{136}Xe. Our computed results for the CC neutrino and antineutrino reactions are shown in Figs. 1 and 2, respectively. Similarly, the results for the NC electron-neutrino scattering are shown in Fig. 3. In the aforementioned figures we also display for each multipole the contributions coming from the vector and axial-vector pieces of the nuclear current. Furthermore, the interference contributions which are coming from the mixing between the axial-vector and vector parts are indicated. It is seen in Fig. 1 that as expected the cross section for the CC neutrino scattering is dominated by Gamow-Teller-like transitions to 1^+ final states in the odd-odd nucleus ^{136}Cs. Fermi-like (0^+) and spin-dipole-like (2^-) transitions contribute also significantly. For the antineutrino reaction (7) the contributions

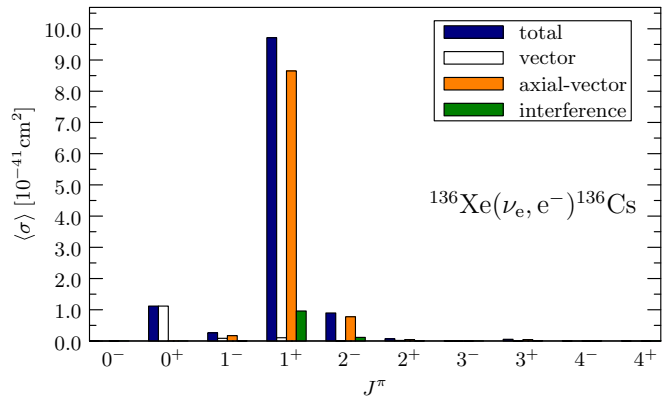

FIG. 1. (Color online) Contributions from the dominant multipole channels to the averaged cross section for the CC neutrino scattering off ^{136}Xe.

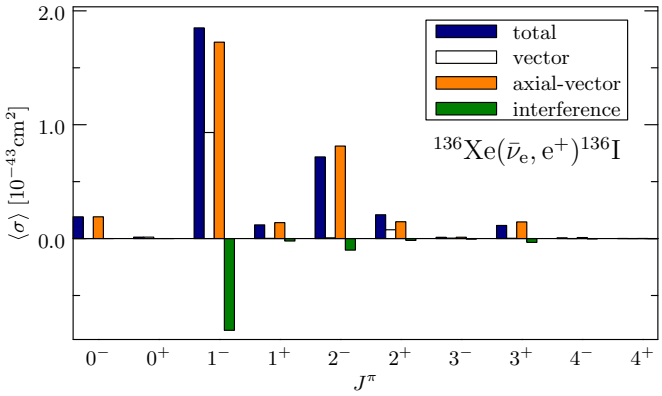

FIG. 2. (Color online) Same as Fig. 1 but for the CC antineutrino scattering.

coming from the 0^+ and 1^+ multipoles are largely suppressed because of the large neutron excess. Consequently, the 1^- and 2^- transitions are relatively more important for the CC antineutrino scattering; see Fig. 2. Moreover, we can conclude that the NC neutrino scattering off ^{136}Xe is dominated by 1^+ transitions. However, transitions mediated by the 1^- and 2^- multipoles are also important. The aforementioned results are in agreement with the ones which have been found for other nuclei; see, e.g., Ref. [17,35]. For the NC antineutrino reaction (9) the interference term has a different sign compared to the neutrino reaction (8); see Eq. (13). However, the axial-vector and vector contributions are the same as for the neutrino scattering. As is seen in Table VI the nonelectron neutrinos have larger average energies than the electron neutrinos, but the relative contributions coming from the different multipoles are almost the same and the results in Fig. 3 are thus only scaled by a common factor in the case of nonelectron neutrinos.

To understand better how the various nuclear final states contribute to the averaged cross sections we have in addition computed the cumulative sums of the averaged cross sections. These sums are defined by

$$\langle\sigma\rangle_{\rm cum}^{(n)} = \sum_{k=1}^{n}\langle\sigma\rangle_k, \tag{29}$$

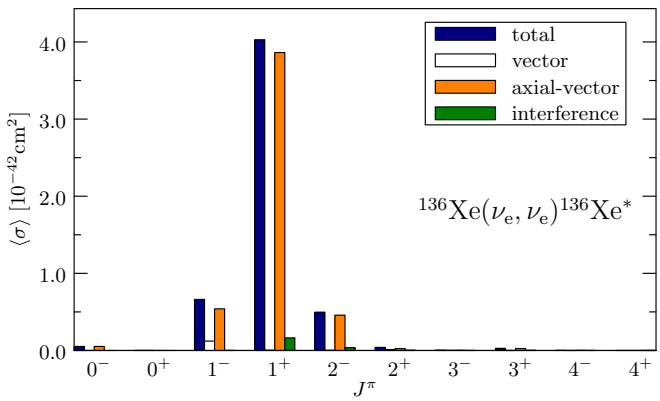

FIG. 3. (Color online) Same as Fig. 1 but for the NC neutrino scattering off ^{136}Xe.

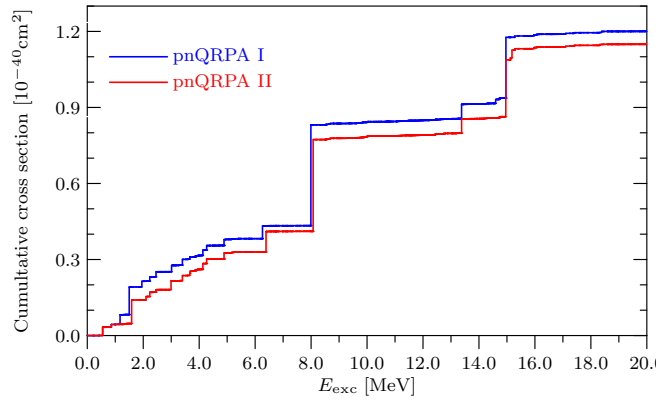

FIG. 4. (Color online) Cumultative sums of the averaged cross section for the charged-current electron-neutrino scattering (6) off ^{136}Xe. Results are shown for the two different pnQRPA calculations which are discussed in the text.

where $\langle\sigma\rangle_k$ denotes the contribution to the averaged cross section coming from the transition to the final state k.

In Fig. 4 are shown the cumulative sums for the CC electron-neutrino scattering off ^{136}Xe. In the figure the results for the two pnQRPA calculations (pnQRPA I and pnQRPA II) are compared with each other. It is seen that a large contribution is arising from a state at about $E_{\rm exc} = 8$ MeV. This contribution is coming from the low-lying satellite of the giant Gamow-Teller resonance. The centroid of the giant Gamow-Teller resonance which is found at 15 MeV contributes also significantly. It is seen in the figure that the largest relative discrepancies between the two pnQRPA calculations are found for the low-lying states, i.e., $E_{\rm exc} \leq 5.0$ MeV. However, the value of $g_{\rm pp}$ also affects the contribution to the cross section coming from the strong state at about $E_{\rm exc} \approx 8$ MeV. Similarly, we display the results for the charged-current electron-antineutrino and the neutral-current electron-neutrino scatterings in Figs. 5 and 6 respectively. We can conclude from Fig. 5 that the antineutrino reaction (7) is dominated by transitions to final states with excitation energies $E_{\rm exc} \leq 10$ MeV. Furthermore, the neutral-current neutrino-nucleus scattering is dominated by a transition of the form $0^+_{\rm g.s.} \longrightarrow 1^+_{12}$ where the state

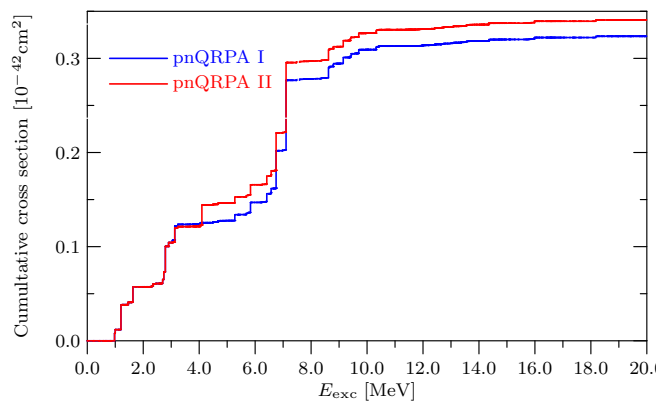

FIG. 5. (Color online) Same as Fig. 4 but for the antineutrino reaction (7).

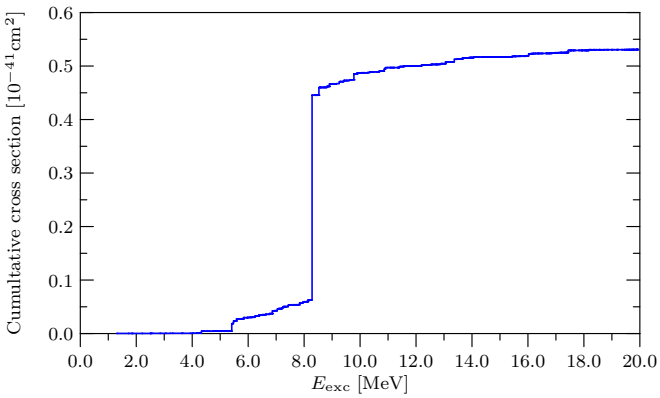

FIG. 6. (Color online) Same as Fig. 4 but for the neutral-current neutrino-nucleus scattering off ^{136}Xe.

1^+_{12} is the giant $M1$ resonance with an excitation energy of $E_{\rm exc} \approx 8.3$ MeV.

It is presumed in the present work that the supernova energy is equally partitioned between the neutrino flavors. The number of CC neutrino scattering events in a detector per kilo-ton (kton) of target mass can then be expressed in the form [19]

$$N_\nu^{\rm CC}(R) = \frac{n_{\rm T}}{4\pi R^2}\int [p(E_{\mathbf{k}})N_{\nu_{\rm e}}F^0_{\nu_{\rm e}}(E_{\mathbf{k}}) + [1-p(E_{\mathbf{k}})]N_{\nu_{\rm x}}F^0_{\nu_{\rm x}}(E_{\mathbf{k}})]\sigma(E_{\mathbf{k}})\mathrm{d}E_{\mathbf{k}}, \quad (30)$$

where $n_{\rm T}$ represents the number of nuclei per kton and R is the distance from the supernova. In Eq. (30) the numbers of electron neutrinos and nonelectron neutrinos are given by

$$N_{\nu_{\rm e}} = \frac{E_{\rm tot}}{6\langle E_{\nu_{\rm e}}\rangle} \quad (31)$$

and

$$N_{\nu_{\rm x}} = \frac{E_{\rm tot}}{6\langle E_{\nu_{\rm x}}\rangle}, \quad (32)$$

where $E_{\rm tot}$ is the total energy which is emitted as neutrinos. The generalization of Eq. (30) to the case of antineutrinos is straightforward.

Correspondingly, the number of NC events can be written as

$$N_\nu^{\rm NC}(R) = \frac{n_{\rm T}}{4\pi R^2}(N_{\nu_{\rm e}}\langle\sigma\rangle_{\nu_{\rm e}} + 2N_{\nu_{\rm x}}\langle\sigma\rangle_{\nu_{\rm x}}). \quad (33)$$

In Fig. 7 are shown the expected number of CC and NC neutrino-nucleus scattering events as functions of the distance R to the supernova. The corresponding results for the antineutrino scattering are displayed in Fig. 8. In the present calculations a total energy of $E_{\rm tot} = 3.0 \times 10^{53}$ ergs has been adopted. In the aforementioned figures we show for the CC scattering the results for nonoscillating neutrinos (antineutrinos) and for (anti)neutrinos which have undergone flavor conversions for the normal and inverted mass hierarchy cases. We can conclude from Fig. 7 that for a typical galactic supernova (i.e., $R \approx 10$ kPc) several hundreds of CC events are expected for a detector consisting of 1 kton of ^{136}Xe. For the antineutrino scattering most of the events are neutral-current

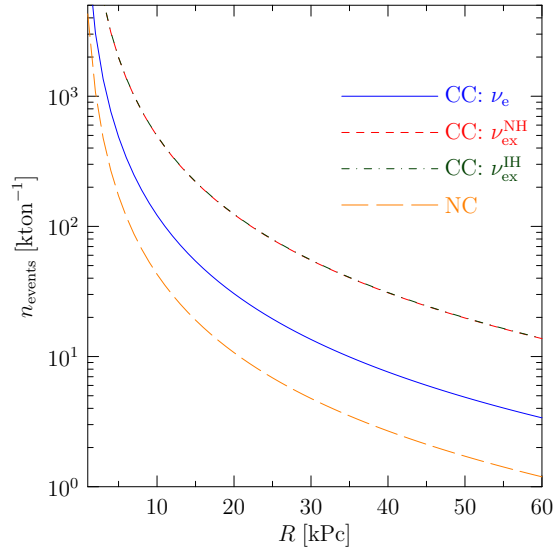

FIG. 7. (Color online) The number of expected CC and NC neutrino scattering events per kiloton of ^{136}Xe as functions of the distance from the supernova.

ones because of the large suppression of the CC antineutrino cross sections.

From Figs. 7 and 8 it can be concluded that the events in a detector based on ^{136}Xe will be mainly caused by CC neutrino-nucleus scatterings. Furthermore, for the adopted prescription for the neutrino mixing, one has that $p(E_{\mathbf{k}}) = 0$ in the case of normal mass hierarchy. The expression for the yield (i.e., number of events per kiloton) is then simply

$$N_\nu^{\rm CC}(R) = \frac{n_{\rm T}}{4\pi R^2}N_{\nu_x}\langle\sigma\rangle_{\nu_{\rm x}} = \frac{n_{\rm T}(E_{\rm tot}/6)}{4\pi R^2} \times \frac{\langle\sigma\rangle_{\nu_{\rm x}}}{\langle E_{\nu_x}\rangle}. \quad (34)$$

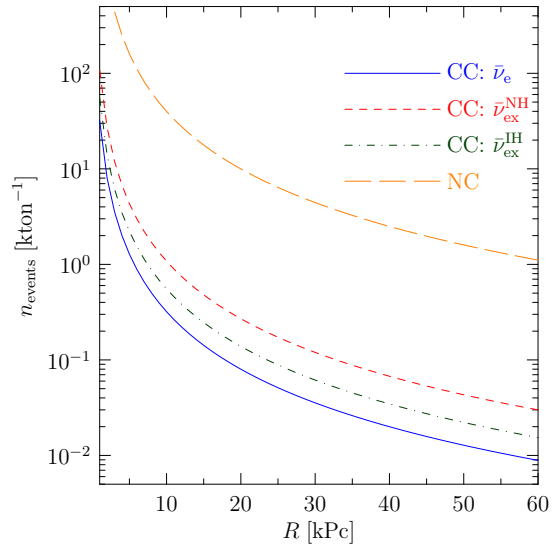

FIG. 8. (Color online) The number of expected CC and NC antineutrino scattering events per kiloton of ^{136}Xe as functions of the distance from the supernova.

TABLE IX. Averaged cross sections in units of 10^{-40} cm^2 and the number of events produced in an earth-bound detector per kton of ^{136}Xe for $\langle E_{\mathbf{k}}\rangle = 15.0,\ 16.3,\ 20.0$ MeV and $\alpha = 0.0,\ 2.0$.

$(\langle E_{\mathbf{k}}\rangle,\alpha_\nu)$	$\langle\sigma\rangle$	N_ν^{CC}
(15.0,0.0)	3.78	291
(15.0,2.0)	3.31	255
(16.3,0.0)	4.87	345
(16.3,2.0)	4.28	303
(20.0,0.0)	8.56	495
(20.0,2.0)	7.86	454

The above expression is also valid in the case of the inverted mass hierarchy to a good approximation because the cross section $\sigma(E_{\mathbf{k}})$ is rather small for $E_{\mathbf{k}} < E_s = 7.0$ MeV. The neutrino spectra of the nonelectron neutrinos are, however, rather uncertain. Depending on the chosen supernova model the average energy can vary between 15 and 20 MeV; see, e.g., Ref. [36]. For this reason we have also studied the sensitivity of the charged-current neutrino responses and the expected number of events in an earth-bound detector (34) on the average neutrino energy $\langle E_{\mathbf{k}}\rangle$ and the parameter α_ν. In Table IX the results for $\langle E_{\mathbf{k}}\rangle = 15.0,\ 16.3,\ 20.0$ MeV and $\alpha = 0.0,\ 2.0$ are compared with each other. In the table the results for the number of events are given for a supernova at the distance $R = 10$ kPc with the total energy $E_{\mathrm{tot}} = 3.0 \times 10^{53}$ ergs. It is seen in Table IX that the computed numbers of events vary by a factor of almost two, depending on the adopted values of $\langle E_{\mathbf{k}}\rangle$ and α_ν. The results in the table are exact for the chosen prediction for $p(E_{\mathbf{k}})$ in the case of normal mass hierarchy. For the inverted mass hierarchy the results are modified by about 1%.

V. CONCLUSIONS

In this work we have performed a study of the charged-current and neutral-current (anti)neutrino-nucleus scatterings off ^{136}Xe. The cross sections have been computed for energies of the incoming lepton, which are relevant for supernova neutrinos. The neutrino-nucleus responses have also been computed by folding the cross sections with appropriate energy spectra for supernova neutrinos. In the present work the nuclear wave functions for the states in ^{136}Xe have been constructed by using the QRPA. Similarly, the pnQRPA has been used to compute the states in the β-decay partners ^{136}Cs and ^{136}I.

We have also in this paper studied the impact of neutrino-flavor transformations on the computed flux-averaged cross sections by adopting a specific choice of the final energy spectra of the supernova (anti)neutrinos. We have for this particular case found that the charged-current neutrino and antineutrino flux-averaged cross sections are significantly modified by neutrino-flavor transformations. According to our calculations the charged-current neutrino cross sections are almost independent of the mass hierarchy. Because of the relatively simple treatment of the neutrino-flavor conversions, our results should only be considered as rough estimates of how the nuclear responses could be modified by collective neutrino oscillations and neutrino-matter interactions occurring under certain supernova conditions. Computations of more accurate estimates of the neutrino signal produced in an earth-bound detector by supernova neutrinos requires the use of more sophisticated treatments of neutrino mixing, which is beyond the scope of the present work.

As expected, we have found in this work that most of the events in an earth-bound detector will be caused by charged-current neutrino scatterings. Contrary to this, the antineutrinos will mostly cause neutral-current reactions because of the large suppression of the charged-current antineutrino channel.

The results which have been computed in this paper show that for the charged-current and neutral-current neutrino scatterings the most crucial transitions are the ones which are mediated by the 1^+ multipole. However, for the charged-current antineutrino channel the 1^+ transitions are largely suppressed. Therefore, spin-dipole-like transitions mediated by the 1^- and 2^- multipoles are the most important ones. These results are similar to the ones which have been obtained for other nuclear systems.

Furthermore, we have found in the present work that the computed averaged cross sections for the charged-current neutrino and antineutrino scatterings off ^{136}Xe are not very sensitive to the adopted value of the particle-particle strength (g_{pp}) in the 1^+ channel. This means that at least for ^{136}Xe the possible uncertainty of the value of that parameter does not have a crucial effect on the predictions of the nuclear responses to supernova neutrinos.

ACKNOWLEDGMENTS

This work has been supported by the Academy of Finland under the Finnish Center of Excellence Program 2012–2017 (Nuclear and Accelerator Based Program at JYFL). We also thank the 973 Program of China (Grant No. 2013CB834401), the National Natural Science Foundation of China (Grant No. 11225524), and Shanghai Key Laboratory (Grant No. 11DZ2260700) for financial support.

[1] G. G. Raffelt, Prog. Part. Nucl. Phys. **64**, 393 (2010).
[2] G. G. Raffelt, Ann. Rev. Nucl. Part. Sci. **49**, 163 (1999).
[3] K. Scholberg, Ann. Rev. Nucl. Part. Sci. **62**, 81 (2012).
[4] P. D. Serpico, S. Chakraborty, T. Fischer, L. Hüdepohl, H. T. Janka, and A. Mirizzi, Phys. Rev. D **85**, 085031 (2012).
[5] A. Dighe, J. Phys. Conf. Ser. **136**, 022041 (2008).
[6] B. Dasgupta, A. Dighe, G. G. Raffelt, and A. Y. Smirnov, Phys. Rev. Lett. **103**, 051105 (2009).
[7] K. Langanke and G. Martínez-Pinedo, Rev. Mod. Phys. **75**, 819 (2003).
[8] K. Langanke and E. Kolbe, At. Data Nucl. Data Tables **79**, 293 (2001).
[9] HALO Helium and Lead Observatory, http://www.snolab.ca/halo/.
[10] H. Ejiri *et al.*, Eur. Phys. J. Special Topics **162**, 239 (2008).
[11] Hyper-Kamiokande, http://www.hyperk.org/.

[12] J. Suhonen and O. Civitarese, Phys. Rep. **300**, 123 (1998).
[13] M. Auger *et al.*, Phys. Rev. Lett. **109**, 032505 (2012).
[14] EXO Enriched Xenon Observatory, https://www-project.slac.stanford.edu/exo/.
[15] J. S. O'Connell, T. W. Donnelly, and J. D. Walecka, Phys. Rev. C **6**, 719 (1972).
[16] E. Ydrefors and J. Suhonen, Adv. High Energy Phys. **2012**, 373946 (2012).
[17] E. Ydrefors, K. G. Balasi, T. S. Kosmas, and J. Suhonen, Nucl. Phys. A **896**, 1 (2012).
[18] E. Ydrefors and J. Suhonen, Phys. Rev. C **87**, 034314 (2013).
[19] W. Almosly, E. Ydrefors, and J. Suhonen, J. Phys. G: Nucl. Part. Phys. **40**, 095201 (2013).
[20] J. Suhonen, *From Nucleons to Nucleus: Concepts of Microscopic Nuclear Theory* (Springer, Berlin, 2007).
[21] J. Suhonen and O. Civitarese, Nucl. Phys. A **924**, 1 (2014).
[22] E. Ydrefors *et al.*, in *Neutrinos: Properties, Reactions, Sources, and Detection*, edited by J. P. Greene (Nova Science, New York, 2011).
[23] J. Engel, Phys. Rev. C **57**, 2004 (1998).
[24] J. D. Walecka, *Theoretical Nuclear and Subnuclear Physics* (Imperial College Press, London, 2004).
[25] A. Bohr and B. R. Mottelson, *Nuclear Structure* (Benjamin, New York, 1969), Vol. 1.
[26] K. Holinde, Phys. Rep. **68**, 121 (1981).
[27] P. Puppe *et al.*, Phys. Rev. C **84**, 051305(R) (2011).
[28] O. Civitarese and J. Suhonen, Phys. Rev. C **89**, 044319 (2014).
[29] W. Almosly, B. G. Carlsson, J. Dobaczewski, J. Suhonen, J. Toivanen, P. Vesely, and E. Ydrefors, Phys. Rev. C **89**, 024308 (2014).
[30] H. Duan, G. M. Fuller, and Y.-Z. Qian, Annu. Rev. Nucl. Part. Sci. **60**, 569 (2010).
[31] H. Duan and J. P. Kneller, J. Phys. G: Nucl. Part. Phys. **36**, 113201 (2009).
[32] B. Dasgupta and A. Dighe, Phys. Rev. D **77**, 113002 (2008).
[33] G. Martínez-Pinedo, B. Ziebarth, T. Fischer, and K. Langanke, Eur. Phys. J. A **47**, 98 (2011).
[34] S. Chakraborty, S. Choubey, S. Goswami, and K. Kar, JCAP 06 (2010) 007.
[35] R. Lazauskas and C. Volpe, Nucl. Phys. A **792**, 219 (2007).
[36] M. T. Keil and G. G. Raffelt, Astrophys. J. **590**, 971 (2003).